

Green Chemistry

Accepted Manuscript



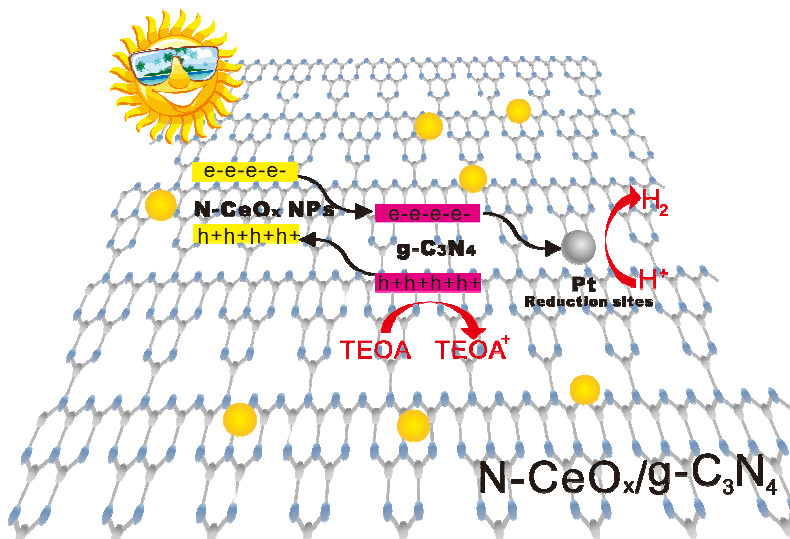
This is an *Accepted Manuscript*, which has been through the Royal Society of Chemistry peer review process and has been accepted for publication.

Accepted Manuscripts are published online shortly after acceptance, before technical editing, formatting and proof reading. Using this free service, authors can make their results available to the community, in citable form, before we publish the edited article. We will replace this *Accepted Manuscript* with the edited and formatted *Advance Article* as soon as it is available.

You can find more information about *Accepted Manuscripts* in the [Information for Authors](#).

Please note that technical editing may introduce minor changes to the text and/or graphics, which may alter content. The journal's standard [Terms & Conditions](#) and the [Ethical guidelines](#) still apply. In no event shall the Royal Society of Chemistry be held responsible for any errors or omissions in this *Accepted Manuscript* or any consequences arising from the use of any information it contains.

Graphic Abstract



Nitrogen-doped CeO_x nanoparticles modified $\text{g-C}_3\text{N}_4$ was successfully prepared via a one-pot method, showing greatly enhanced photocatalytic activity for hydrogen generation under visible light when compared to the pure $\text{g-C}_3\text{N}_4$ photocatalyst.

Cite this: DOI: 10.1039/c0xx00000x

www.rsc.org/xxxxxx

ARTICLE TYPE

Nitrogen-doped CeO_x Nanoparticles Modified Graphitic Carbon Nitride for Enhanced Photocatalytic Hydrogen Production

Jie Chen^a, Shaohua Shen^{*a}, Po Wu^a, Liejin Guo^{*a}

Received (in XXX, XXX) Xth XXXXXXXXX 20XX, Accepted Xth XXXXXXXXX 20XX

DOI: 10.1039/b000000x

Nitrogen-doped CeO_x nanoparticles (N-CeO_x NPs) were directly formed on graphitic carbon nitride (g-C₃N₄) via a facile one-pot method by annealing the mixture of Ce(NO₃)₃ and melamine as CeO_x and g-C₃N₄ precursors, respectively. Nitrogen was in-situ doped into CeO_x in the NH₃ atmosphere released by melamine decomposition during annealing process. The physical and photophysical properties of N-CeO_x NPs modified g-C₃N₄ photocatalysts were investigated to reveal the effects of N-CeO_x NPs on the photocatalytic activities of g-C₃N₄. It was found that the one-pot annealing method was favorable for forming intimate interfacial contact between N-CeO_x and g-C₃N₄. The visible light photocatalytic hydrogen production activity over g-C₃N₄ was enhanced by ca. 1.2 times with N-CeO_x NPs modification. The great enhancement in photocatalytic performance for the N-CeO_x/g-C₃N₄ heterojunction should be mainly because of the promoted charge transfer and charge separation between N-CeO_x NPs and g-C₃N₄ as resulted from the intimate interfacial contact and Type II band alignment. Additionally, the improved visible light absorption of N-CeO_x NPs induced by nitrogen doping could be another reason for the enhanced photocatalytic activity of the N-CeO_x/g-C₃N₄ heterojunction.

Introduction

Photocatalytic water splitting to produce hydrogen over semiconductors by solar irradiation has received considerable attention due to its potential applications to alleviate global energy crisis and environmental pollution. The development of efficient photocatalysts utilizing visible light (~43% of the solar spectrum) is of vital importance to fulfill practical application of this technique. H₂ production under visible light irradiation has been demonstrated with myriad of semiconductor photocatalysts,¹⁻³ including oxides, sulfides, oxynitrides, et al. However, some intrinsic drawbacks, such as poor optical absorption ability (e.g., TiO₂,⁴ ZnO⁵) for wide band gap oxides, poor photochemical stability for sulfides (e.g., CdS⁶), and complicated preparation process for oxynitrides (e.g., GaN:ZnO⁷) still greatly limit their practical application for photocatalytic solar-hydrogen conversion. To address these limitations, novel photocatalytic materials with efficient visible light absorption and good photochemical stability as well as facile preparation method must be developed for practical application of this state-of-the-art technique.

Since the first demonstration by Wang et al.,⁸ the novel metal-free polymer n-type semiconductor prepared by simply annealing the cheap and abundant precursors (urea, melamine, dicydiamide, cyanamide, et al.), namely layered carbon nitride with a graphitic structure (g-C₃N₄), has attracted extensive interest for its proper band gap (E_g ~ 2.7 eV) and excellent photocatalytic stability.⁹ However, due to the poor optical absorption above 460 nm and the fast recombination of photogenerated electron-hole pairs, the

photocatalytic efficiency of pure g-C₃N₄ was relatively low. To enhance its photocatalytic performance, different methods have been exploited, including creating porous structures,¹⁰ doping with metal¹¹ or non-metal ions,¹² combining with other semiconductors¹³ and loading co-catalysts.¹⁴ Among them, combining g-C₃N₄ with other semiconductors to form semiconductor/g-C₃N₄ composite photocatalysts has been most widely studied. Many kinds of nanocomposites such as BiOBr/g-C₃N₄,¹³ TiO₂/g-C₃N₄,¹⁵ ZnO/g-C₃N₄,¹⁶ Fe₂O₃/g-C₃N₄,¹⁷ and Ag₂O/g-C₃N₄¹⁸ have been developed for the improved charge separation and/or enhanced visible light absorption, leading to higher photocatalytic activities than pure g-C₃N₄.

As one of the reactive rare earth oxides with outstanding catalytic properties, CeO_x has been widely used in solar cells, photocatalytic degradation of dye pollutants and hydrogen evolution.^{19,20} By far, various kinds of heterojunctions formed between CeO_x and other semiconductors (e.g., TiO₂,²¹ Cu₂O,²² BiVO₄,²³ CdS,²⁴ etc.) have been developed with enhanced photocatalytic performances due to the improved charge separation ability. However, in these CeO_x/semiconductor composite photocatalysts, CeO_x could only act as a Type II band alignment counterpart to improve the charge separation but not as a visible light sensitizer due to its large band gap (E_g ~ 2.9 eV) limiting its optical absorption in visible light region. Nitrogen doping was a widely accepted approach to enhance the visible light response of CeO_x as well as other wide band gap metal oxides.^{4,25,26} Mao et al.²⁵ synthesized nitrogen doped CeO_x (N-CeO_x) through a wet-chemical route, the optical property of CeO_x was much improved and then the visible-light photocatalytic

performance for methylene blue decomposition was enhanced. Jorge et al.²⁶ prepared porous nitrogen doped CeO_x with effective visible light-active performance for the decomposition of acetaldehyde by annealing mesoporous nanocrystalline ceria under NH₃ at 550-700 °C. Note that g-C₃N₄ can be easily synthesized from various simple precursors via a polycondensation reaction at around 500-600 °C with NH₃ released.^{27,28} It becomes highly possible to dope nitrogen into the lattice of the semiconductors to form N-semiconductor/g-C₃N₄ heterojunction by heating the mixture precursors of semiconductors and g-C₃N₄.²⁹⁻³¹ However, as far as we know, N-CeO_x/semiconductor composite photocatalysts with N-CeO_x acting as an effective visible-light sensitizer have not been reported yet.

In the present study, we successfully prepared a series of nitrogen doped CeO_x nanoparticles (N-CeO_x NPs) modified g-C₃N₄ photocatalysts via a facile one-pot method by simply heating the mixture of Ce(NO₃)₃ and melamine as CeO_x and g-C₃N₄ precursors under 550 °C. The effect of N-CeO_x NPs on the optical absorption and charge carrier separation, and then the enhanced photocatalytic activities of g-C₃N₄ were investigated in detail.

Experimental Details

Synthesis Procedure

All chemicals in the present study are of analytical grade and used as received without further purification. N-CeO_x NPs modified g-C₃N₄ photocatalysts were prepared by a facile one-pot method as illustrated in Fig S1. Typically, 3.0 g of melamine and V mL (V = 1, 3, 5, 7, 10, 15) of 0.031 g/mL Ce(NO₃)₃•6H₂O aqueous solution were added into 200 mL of distilled water, and heated at 90 °C for 1 h under stirring, the temperature was then raised to 100 °C for complete water evaporation. The resulting mixture was put into an alumina crucible with a cover, and annealed at 550 °C under Ar flow (30 mL/min) for 4 h with ramping rate of 20 °C/min. g-C₃N₄ modified with different amounts of N-CeO_x NPs by adding V mL of 0.031 g/mL Ce(NO₃)₃•6H₂O aqueous solution is denoted as Ce-CN-V (V = 1, 3, 5, 7, 10, 15).

Pure g-C₃N₄ and CeO_x was prepared by the same process without adding Ce(NO₃)₃ or melamine. Ce-CN-M composite as reference was prepared by mechanical mixing of CeO_x and pure g-C₃N₄. Ce-CN-T composite was also prepared as reference by the two-step method, namely, annealing the grounded mixture of melamine and pure CeO_x following the same heating process as described above. To be consistent with the loading amount of CeO_x in Ce-CN-5, CeO_x used for preparing Ce-CN-M and Ce-CN-T was obtained by heating and then annealing 5 mL of 0.031 g/mL Ce(NO₃)₃•6H₂O aqueous solution at 550 °C. In addition, reference samples of Ce-CN-M₂ and Ce-CN-T₂ were also prepared following the same preparation procedure as Ce-CN-M and Ce-CN-T, respectively, while using 15 mL of Ce(NO₃)₃•6H₂O aqueous solution as the CeO_x precursors in order to be consistent with the loading amount of CeO_x in Ce-CN-15.

Characterization

The transmission electron microscopy (TEM) images were obtained from a FEI Tecnai G2 F30 transmission electron

microscope at an accelerating voltage of 300 kV. The X-ray diffraction (XRD) patterns were obtained from a PANalytical X'pert MPD Pro diffractometer operated at 40 kV and 40 mA using Ni-filtered Cu K α irradiation (Wavelength 1.5406 Å). UV-vis absorption spectra (UV-vis) were measured on a HITACHI U4100 instrument equipped with labsphere diffuse reflectance accessory. Photoluminescence spectra (PL, including steady and time-resolved fluorescence emission) were carried out at room temperature on a PTI QM-4 fluorescence spectrophotometer. X-ray photoelectron spectroscopy (XPS) data were obtained on a Kratos Axis-Ultra DLD instrument with a monochromatized Al K α line source (150 W). All binding energies were referenced to the C 1s peak at 284.8 eV.

Photocatalytic Activity Evaluation

Photocatalytic hydrogen evolution was performed in a gas-closed circulation system with a 230 mL Pyrex cell as the photoreactor. A 300 W Xe lamp was used as the light source, and the UV part of irradiated light was removed by a 420-nm cutoff filter. Hydrogen evolved was analyzed on a thermal conductivity detector (TCD) gas chromatograph (NaX zeolite column, N₂ as a carrier gas) every 60 min. In a typical experiment, the photocatalyst powder (50 mg) was dispersed in 200 mL of 10 vol% triethanolamine (TEOA) aqueous solution under stirring. Pt (1 wt%) was photodeposited in situ on the photocatalysts from the precursor of H₂PtCl₆•6H₂O. Nitrogen was purged through the reactor for 15 min before photocatalytic reaction to remove oxygen. The temperature for all the photocatalytic reactions was kept at 35 ± 0.5 °C by thermostatic water bath.

Results and Discussion

Fig. 1 shows the TEM images of the as-prepared Ce-CN-V (V = 1, 5, 10) photocatalysts. g-C₃N₄ photocatalyst exhibits a layered structure as shown in Fig. 1A-C, which offered good substrate for loading N-CeO_x NPs. As demonstrated in Fig. 1A, for the Ce-CN-1 photocatalyst, N-CeO_x NPs were dispersed evenly on g-C₃N₄ with a size range of 7-17 nm (See Fig. S2 in ESI† for the particle size distribution). With the volume of the Ce(NO₃)₃ precursor solution increased to 5 mL, more N-CeO_x NPs were found on the surface of g-C₃N₄ (Fig. 1B). Despite of aggregation, no bulk CeO_x was found on g-C₃N₄ and the particle size distribution of Ce-CN-5 was almost the same with that of Ce-CN-1, as evidenced in Fig. S2. Further increasing the volume of Ce(NO₃)₃ precursor solution gave rise to more aggregates of N-CeO_x NPs, covering larger areas of g-C₃N₄ surface, as observed for Ce-CN-10 (Fig. 1C). It was reported that the shading effect induced by nanoparticle aggregation was detrimental for the photocatalytic hydrogen production reaction by covering the active species at the photocatalyst's surface.^{32,33} As shown in Fig. 1D, the fringe spacings of N-CeO_x in Ce-CN-5 were measured to be 3.18 Å and 1.96 Å, corresponding to the (111) and (220) lattice planes of cubic CeO_x, respectively, which are a little larger than the reported values of (111) and (220) lattice planes of cubic CeO_x (3.12 Å and 1.91 Å, JCPDS 004-0593). This is very likely because that nitrogen was introduced into the crystal lattice of CeO_x, and thus the lattice parameters of nitrogen doped CeO_x in Ce-CN-V nanocomposites became larger than those of pure CeO_x, due to the substitution of 4-coordinated O²⁻ (ionic radius : 1.38 Å) by N³⁻ (ionic radius: 1.46 Å) in CeO_x.³⁴

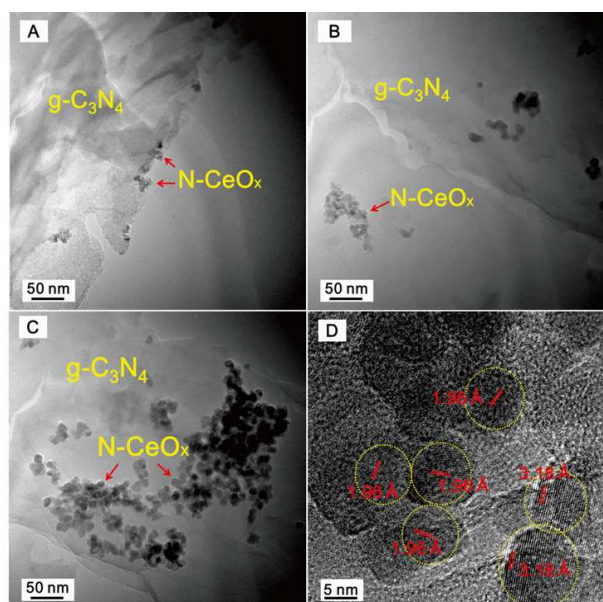


Fig.1 TEM images of Ce-CN-V photocatalysts: (A) V=1, (B) V=5, (C) V=10, (D) The magnified TEM image of Ce-CN-5.

X-ray diffraction (XRD) patterns for $g\text{-C}_3\text{N}_4$, CeO_x and Ce-CN-V photocatalysts were taken to investigate their crystal structures. As shown in Fig. 2A, the (100) peak at $2\theta = 13.0^\circ$ corresponding to d value of 0.676 nm is related to an in-plane structural packing motif of $g\text{-C}_3\text{N}_4$, such as the hole-to-hole distance of the nitride pores in the crystal.³⁵ Both pure $g\text{-C}_3\text{N}_4$ and Ce-CN-V nanocomposites show a strong characteristic (002) peak at $2\theta = 27.4^\circ$, corresponding to the interlayer-stacking of the conjugated aromatic system with a stacking distance of 0.326 nm, indicating that the as-prepared nanocomposites possess layered structures of $g\text{-C}_3\text{N}_4$. It was also found that with increased N- CeO_x amounts in the nanocomposites, the relative intensity of both (100) and (002) peaks were significantly decreased, maybe due to the deposition of N- CeO_x onto the surface of $g\text{-C}_3\text{N}_4$.¹³ Here, the weakening of the (100) peak could be attributed to that the nitride pores were slightly distorted with N- CeO_x modification and then the hole to hole distance was changed.^{35,36} While for the (002) peak, the weakening could be resulted from a decrease in structural correlation length induced by the introduction of small sized N- CeO_x NPs.^{37,38}

The XRD peaks of pure CeO_x were in good agreement with the cubic phase of CeO_x (JCPDS 004-0593). For the Ce-CN-V nanocomposites, with the volume of $\text{Ce}(\text{NO}_3)_3$ precursor solution increasing, the CeO_x diffraction peaks gradually appeared and became stronger, indicating more N- CeO_x NPs presented in the nanocomposites. However, as shown in Fig. 2B, the XRD peaks at $2\theta = 28.6^\circ$, 33.1° , 47.5° for CeO_x slightly shifted to lower angle for Ce-CN-V, which should be attributed to the substitution of 4-coordinated O^{2-} (ionic radius: 1.38 Å) by N^{3-} (ionic radius: 1.46 Å) in CeO_x .³⁴ This is understandable because the nitrogen doping happened to CeO_x NPs obtained by annealing $\text{Ce}(\text{NO}_3)_3$ precursor in the NH_3 atmosphere^{25,26} created by heating melamine at 550°C , as described in Fig. S1 and S3 in ESI†. In addition, when compared with the reference samples of Ce-CN-T₂, Ce-CN-M₂, these three XRD peaks also slightly shifted to lower angle for Ce-CN-15, as shown in Fig. S4 in ESI†. These results could help

distinguish the N- CeO_x NPs modified $g\text{-C}_3\text{N}_4$ from $\text{CeO}_x/g\text{-C}_3\text{N}_4$ composites, again indicating that the one-pot method was favorable for nitrogen doping into the lattice of CeO_x , as compared to the mechanical mixing or two-step method.

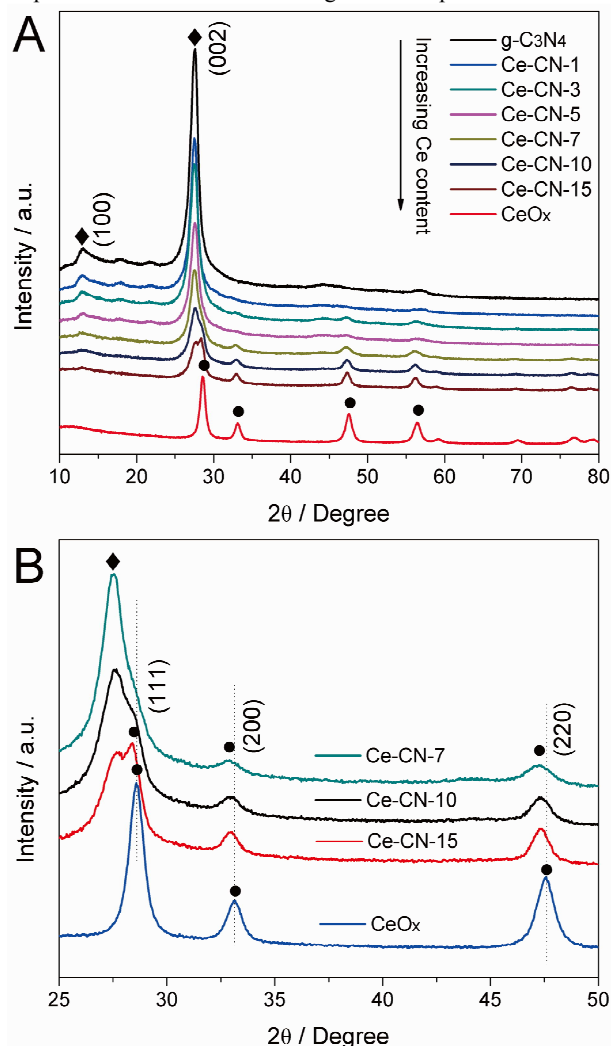


Fig.2 (A) XRD patterns of $g\text{-C}_3\text{N}_4$, CeO_x and Ce-CN-V photocatalysts with various volumes of $\text{Ce}(\text{NO}_3)_3$ precursor solution; (B) XRD patterns of CeO_x , Ce-CN-V ($V = 7, 10, 15$) in the range of $2\theta = 25\text{-}50^\circ$. (◆) and (●) were denoted to mark the characteristic peaks of $g\text{-C}_3\text{N}_4$ and CeO_x , respectively.

As determined by the XPS analysis (Fig. S5), the actual weight ratios of Ce in Ce-CN-V ($V = 1, 3, 5, 7, 10, 15$) were determined to be 0.95, 2.45, 4.22, 5.88, 8.52 and 12.82 wt%, respectively. The weight contents for all the elements (C, N, O, Ce) in $g\text{-C}_3\text{N}_4$ and Ce-CN-V were also calculated and listed in Table S1 in ESI†. Ce 3d XPS spectra of pure CeO_x (Fig. 3a) and Ce-CN-15 (Fig. 3b) were further compared to evidence that nitrogen was introduced to the crystal lattice of CeO_x . As shown in Fig. 3, due to the highly nonstoichiometric nature of CeO_x , both 3+ and 4+ states are present in CeO_x and Ce-CN-5. Note that the Ce 3d binding energies (both Ce^{3+} and Ce^{4+}) of Ce-CN-5 are slightly lower than those of pure CeO_x . For example, the binding energies of $\text{Ce}^{4+} 3d_{3/2}$, $\text{Ce}^{4+} 3d_{5/2}$, $\text{Ce}^{3+} 3d_{3/2}$ and $\text{Ce}^{3+} 3d_{5/2}$ for pure CeO_x are centered at ca. 916.8, 898.1, 900.7 and 882.3 eV, respectively; while those for Ce-CN-5 are located at 916.4, 897.9, 900.4 and

882.0 eV, respectively. Such lower shift in Ce 3d binding energy for Ce-CN-5 should be attributed to an increase in electron density around the Ce cation (Ce-N > Ce-O), which was induced by the replacement of oxygen atoms by nitrogen atoms with lower electronegativity.^{25,39}

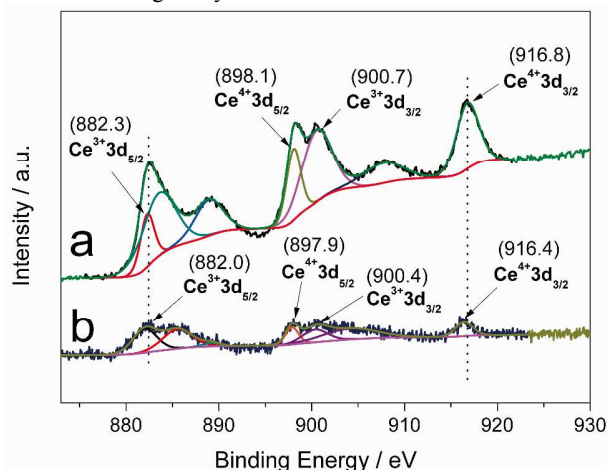


Fig.3 Ce 3d XPS spectra of the (a) CeO_x and (b) Ce-CN-15 photocatalysts.

Fig. 4 shows UV-vis absorption spectra to evaluate the optical absorption properties of the as-prepared photocatalysts. As calculated by the Kubelka–Munk method,^{40,41} the absorption edges of pure g-C₃N₄ and CeO_x at about 460 nm and 430 nm corresponds to band gaps of 2.70 eV and 2.90 eV, respectively. The narrowed band gap and band position fine-tuning of CeO_x by nitrogen doping was also confirmed by DFT calculation (see Computational Methods and Fig. S6 in ESI†). By forming nanocomposites, the absorption edge showed gradual red shift to 490 nm for Ce-CN-15 with increasing N-CeO_x loading amounts. It was also found that the light absorption in the range of $\lambda > 500$ nm was obviously enhanced, mainly due to the nitrogen doping induced significant increase of the light absorption above 500 nm.^{25,26,34} The enhanced visible light absorption was beneficial for the photocatalytic performance as widely reported.^{17,18} However, for the Ce-CN-V (V = 1, 3, 5, 7, 10, 15) photocatalysts, the increasing N-CeO_x loading amounts, which could gradually enhance the visible light absorption, would give rise to more and more serious shading effect^{32,33,41} and hence offset the benefit of the light absorption of N-CeO_x. As a result, this negative shading effect induced by excessive loading of N-CeO_x NPs leads to decreased photocatalytic activity for hydrogen production, as verified by the hydrogen production evaluation of the Ce-CN-V photocatalysts in the later sections.

It was also noted that the visible light absorption of Ce-CN-5 was greatly enhanced compared to Ce-CN-T or Ce-CN-M (See Fig. S7 in ESI†), especially in the range of $\lambda > 500$ nm. This should be attributed to that nitrogen was hardly introduced into the lattice of CeO_x by the two-step method or the mechanical method, and thus the visible light absorption ability of Ce-CN-5 with N-CeO_x modification was much stronger than Ce-CN-T or Ce-CN-M with only CeO_x modification.

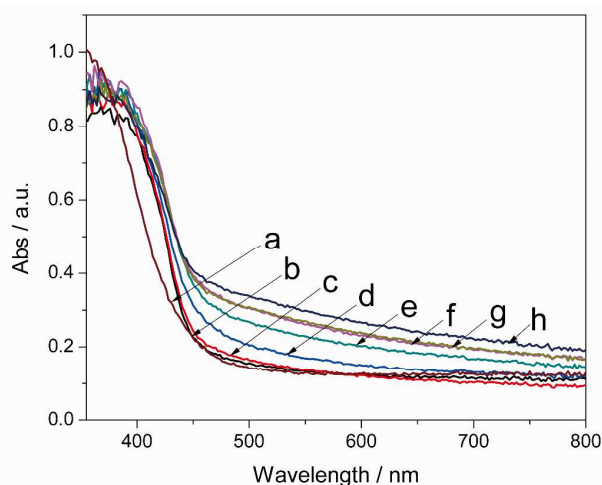


Fig.4 UV-vis diffuse reflectance spectra of the as-prepared photocatalysts. (a) pure CeO_x, (b) g-C₃N₄ and Ce-CN-V photocatalysts with various V: (c) V = 1, (d) V = 3, (e) V = 5, (f) V = 7, (g) V = 10, (h) V = 15.

The photoluminescence (PL) emission spectra are very useful to understand the behavior of photo-generated charge carriers in photocatalysts, since PL emission is resulted from the irradiative recombination of electrons and holes.⁴² Fig. 5A shows the PL spectra for the as-prepared Ce-CN-V photocatalysts. All the photocatalysts exhibited a broad emission peak centered at around 460 nm, and a tail extending to 700 nm. The emission could be attributed to the band-band PL phenomenon related to the recombination of photoinduced electrons and holes in g-C₃N₄.^{41,43} The PL emission intensity exhibits the highest value for pure g-C₃N₄ and decreases monotonously with increasing N-CeO_x contents. This indicates that the recombination of photogenerated charge carriers is inhibited in the Ce-CN-V photocatalysts, due to the photo-induced electron hole pairs are efficiently separated in the N-CeO_x/g-C₃N₄ heterojunctions.

To prove the N-CeO_x/g-C₃N₄ heterojunctions prepared by the one-pot annealing method is superior for charge carriers separation, PL spectra of the reference samples (Ce-CN-T, Ce-CN-M) were also taken for comparison, as shown in Fig. 5B. For the Ce-CN-T photocatalyst prepared by the two-step method, the PL intensity was stronger than that of Ce-CN-5, meaning the poorer charge separation in Ce-CN-T than in Ce-CN-5. This should be due to that the larger size of CeO_x nanoparticles and hence the poorer interfacial contact between CeO_x and g-C₃N₄ (as evidenced in Fig. S8C,D in ESI†) will consequently result in the less efficient charge separation in Ce-CN-T. While for the mechanical mixture sample of Ce-CN-M, the PL emission intensity was even much stronger relative to Ce-CN-T, indicating the very poor charge separation between CeO_x and g-C₃N₄ in Ce-CN-M. This is reasonable, given the serious aggregation of CeO_x nanoparticles and loose interfacial contact between CeO_x and g-C₃N₄ (Fig. S8E,F in ESI†) by simply mechanically mixing CeO_x and g-C₃N₄.

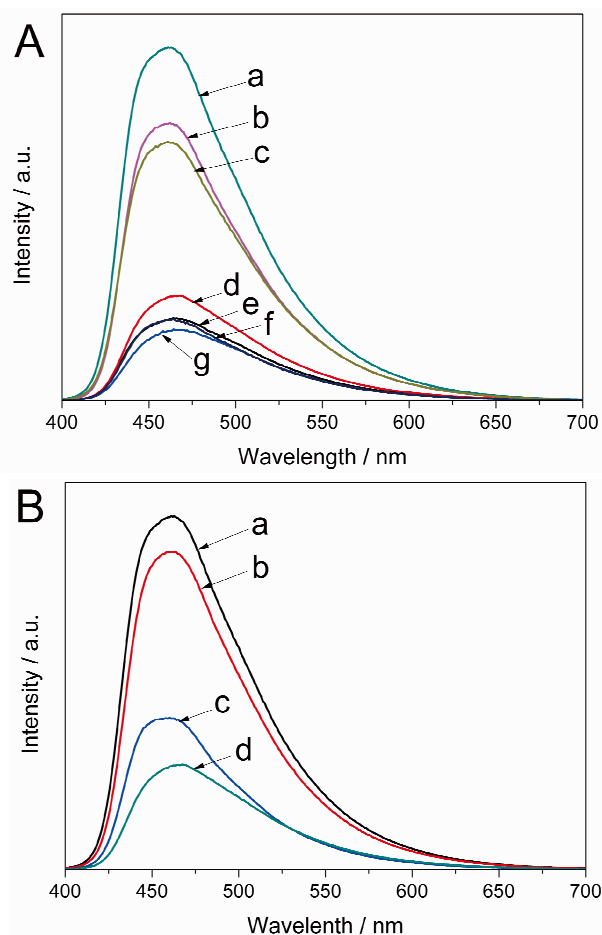


Fig.5 (A) Photoluminescence (PL) spectra of the Ce-CN-V photocatalysts. (a) $g\text{-C}_3\text{N}_4$, (b) Ce-CN-1, (c) Ce-CN-3, (d) Ce-CN-5, (e) Ce-CN-7, (f) Ce-CN-10, (g) Ce-CN-15. (B) PL spectra of (a) $g\text{-C}_3\text{N}_4$, (b) Ce-CN-M, (c) Ce-CN-T, (d) Ce-CN-5.

The charge separation in composite photocatalysts is usually related to the band alignment induced charge transfer at the interfaces of the two components (e.g., type II band alignment).⁴¹ In the present work, the valence band maximum (VBM) edge potentials of CeO_x and $g\text{-C}_3\text{N}_4$ was measured by valence band X-ray photoelectron spectroscopy (VB XPS) to estimate the band alignment for the Ce-CN-V photocatalysts. As shown in Fig. 6, the peak assigned to Ce 4f can be observed at ~ 1.5 eV. It was reported that Ce 4f was accompanied by Ce_2O_3 whereas absent for pure CeO_2 ,⁴⁴ confirming the presence of Ce^{3+} . The band stretching from ca. 3 to 8 eV is assigned to the O 2p orbitals.⁴⁴ For CeO_x , the valence band is derived from the O 2p orbitals, and the band gap of 2.9 eV is derived from O 2p - Ce 4f transition,^{24,44} thus the VBM edge of as-prepared CeO_x is estimated to be about 2.24 eV below the Fermi band (E_f) from the VB XPS spectra. For $g\text{-C}_3\text{N}_4$, the VBM edge is estimated to be 2.36 eV from Fig. 6, in accordance with our previous reports.^{41,43} According to the equation $E_{\text{CB}} = E_{\text{VB}} - E_g$,^{41,45} E_{CB} of CeO_x and $g\text{-C}_3\text{N}_4$ were calculated to be 0.66 eV and 0.32 eV above E_f ,

respectively. Based on the above deduction, as illustrated in Fig. 6, the E_{CB} difference of 0.34 eV could facilitate the electron transfer from the conduction band of CeO_x to that of $g\text{-C}_3\text{N}_4$; while the E_{VB} difference of 0.12 eV will favor hole transfer from the valence band of $g\text{-C}_3\text{N}_4$ to that of CeO_x . Note that due to nitrogen doping in N- CeO_x , the real E_g value for the N- CeO_x must be smaller (dotted line in Fig. 6), as suggested by the improved visible light absorption and DFT calculation results, leading to enhanced visible light response of the nanocomposites photocatalysts of N- $\text{CeO}_x/g\text{-C}_3\text{N}_4$ (e.g., the as-prepared Ce-CN-V heterojunctions).

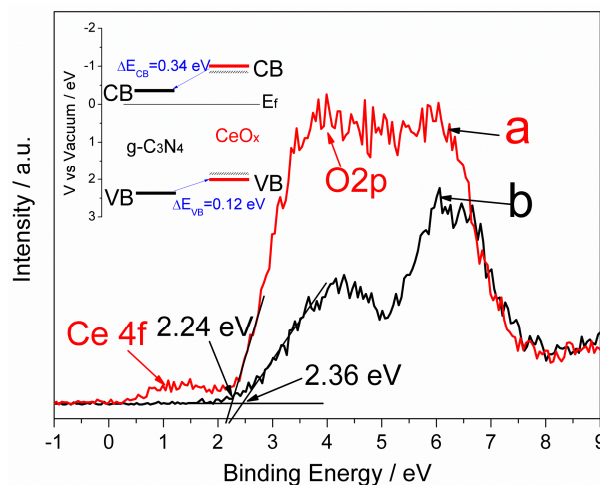


Fig.6 VB XPS spectra for (a): CeO_x and (b): $g\text{-C}_3\text{N}_4$. The inset is the energy band alignment of $\text{CeO}_x/g\text{-C}_3\text{N}_4$ heterojunction. (solid lines: band position for pure CeO_x (red) and $g\text{-C}_3\text{N}_4$ (black); black dotted lines near the CB and VB of CeO_x : estimated band position for N- CeO_x nanoparticles). E_f : fermi level; E_{VB} : valence band energy level; E_{CB} : conduction band energy level.

To further confirm the efficient charge separation between N- CeO_x and $g\text{-C}_3\text{N}_4$ induced by Type II band alignment and intimate interfacial contact, time-resolved fluorescence emission decay spectra of Ce-CN-5, and $g\text{-C}_3\text{N}_4$, Ce-CN-M, Ce-CN-T as references were measured at room temperature as shown in Fig. 7. The kinetic parameters for these as-prepared samples are summarized in Table 1. The average lifetimes of the carriers (τ_{avg}) were determined to be 4.94 ns, 4.99 ns, 9.85 ns and 21.10 ns for $g\text{-C}_3\text{N}_4$, Ce-CN-M, Ce-CN-T and Ce-CN-5, respectively (See decay kinetics calculation in Supporting Information), indicating that the charge recombination in $g\text{-C}_3\text{N}_4$ was effectively inhibited once modified with N- CeO_x (or CeO_x) nanoparticles.^{41,43,45} Especially, the N- $\text{CeO}_x/g\text{-C}_3\text{N}_4$ heterojunction prepared by the one-pot annealing method (Ce-CN-5) showed greatly prolonged carrier lifetime when compared to the reference samples of $g\text{-C}_3\text{N}_4$, Ce-CN-M and Ce-CN-T, again confirming the efficient charge transfer and separation between N- CeO_x and $g\text{-C}_3\text{N}_4$, due to the intrinsic straddling (Type II) band alignment and the intimate interfacial contact.

Cite this: DOI: 10.1039/coxx00000x

www.rsc.org/xxxxxx

ARTICLE TYPE

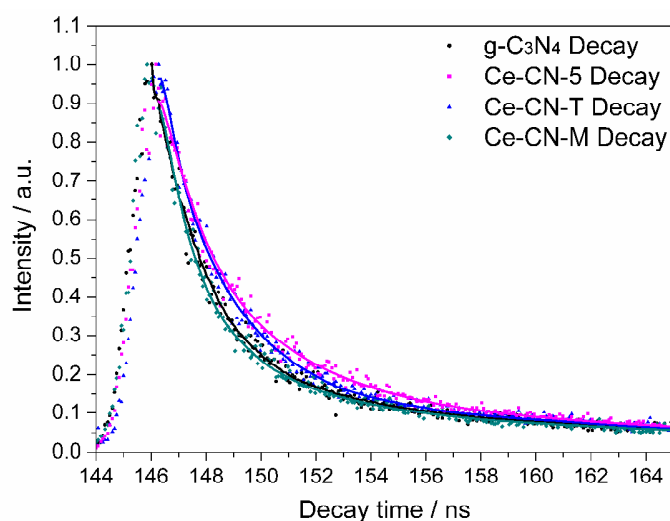


Fig.7 Time-resolved fluorescence emission decay curves for g-C₃N₄, Ce-CN-5, Ce-CN-T and Ce-CN-M at room temperature. Observation wavelength for all the samples was 470 nm and the excitation wavelength was 337 nm. Solid lines represent the kinetic fit using tri-exponential decay analysis

Table 1 Kinetic parameters of the as-prepared samples emission decay analysis.

Samples	A ₁	τ ₁ (ns)	A ₂	τ ₂ (ns)	A ₃	τ ₃ (ns)	τ _{avg} (ns)	χ ²
g-C ₃ N ₄	0.1109	1.425	0.8667	0.033	0.0224	8.558	4.94	0.9571
Ce-CN-M	0.1274	7.929	0.4567	1.410	0.4159	0.343	4.99	0.9606
Ce-CN-T	0.2987	4.122	0.6196	1.207	0.0817	18.69	9.85	1.054
Ce-CN-5	0.2488	2.269	0.1195	25.80	0.6317	0.295	21.10	0.9335

The photocatalytic activity of N-CeO_x NPs modified g-C₃N₄ photocatalysts (Ce-CN-V, V = 1, 3, 5, 7, 10, 15) was evaluated by hydrogen production reaction under visible light ($\lambda > 420$ nm). Pt (1 wt%) was used as the co-catalyst, providing hydrogen evolution sites on the as-prepared photocatalyst for efficient photocatalytic hydrogen production (Fig. S9 in ESI[†]).^{8,46-48}

As shown in Fig. 8A, all the samples are photocatalytically active, while no hydrogen was detected in the absence of either photocatalyst or light irradiation. The rate of hydrogen evolution over pure g-C₃N₄ was 134.5 $\mu\text{mol}\cdot\text{h}^{-1}\cdot\text{g}^{-1}$. With N-CeO_x contents increasing, the photocatalytic activity of Ce-CN-V was greatly improved, with the highest hydrogen evolution rate achieved 292.5 $\mu\text{mol}\cdot\text{h}^{-1}\cdot\text{g}^{-1}$ for Ce-CN-5, which was about 2.2 times that of pure g-C₃N₄. However, the photocatalytic activity was decreased with the further increasing contents of N-CeO_x for Ce-CN-V (V = 7, 10, 15).

To clarify the mechanism for photocatalytic H₂ production over Ce-CN-V, it is necessary to make clear how the N-CeO_x NPs influence the activity of g-C₃N₄, based on three effects resulted from N-CeO_x NPs modification: (1) efficient charge separation between g-C₃N₄ and N-CeO_x induced by the formed Type II band alignment,^{15,16} (2) N-CeO_x acting as visible light sensitizers,^{17,18} (3) the negative shading effect of the excessive N-CeO_x.^{32,33,41} For the Ce-CN-V (V = 1, 3, 5) photocatalysts, as shown from the UV-vis and PL spectra in Fig. 4 and Fig. 5A, both of the visible light absorption and charge separation

efficiency were improved with increasing loading amounts of N-CeO_x NPs, leading to gradual increase in photocatalytic activity for hydrogen evolution. On the other hand, it is noteworthy that both the optical absorption enhancement and the shading effect were related to the N-CeO_x content, that is, the larger the N-CeO_x content, the stronger the two effects. As seen from Fig. 4, the visible light absorption was increased with the increase in the N-CeO_x loading amounts; meanwhile the N-CeO_x NPs aggregated as observed in Fig. 1C, leading to the negative shading effect of aggregated N-CeO_x NPs. Thus, for Ce-CN-V (V = 7, 10, 15), although the light absorption ability was improved by increasing the N-CeO_x loading amounts, the negative shading effect induced by aggregation of N-CeO_x NPs became more significant, leading to the decrease in photocatalytic performances. That is to say, the three factors mentioned above balanced and competed with each other, eventually resulting in the highest photocatalytic performance for the Ce-CN-5 photocatalyst with optimized N-CeO_x loading.

In order to investigate the photocatalytic stability, the photocatalytic experiment for hydrogen production was run for 5 cycles. As shown in Fig. 8B, Ce-CN-5 shows quite good stability for photocatalytic hydrogen production, with hydrogen production rate kept almost unchanged during the 35 h reaction.

Hydrogen production over the reference samples of Ce-CN-M (mechanical mixture) and Ce-CN-T (two-step prepared) was also tested to prove the photocatalytic superiority of N-CeO_x/g-C₃N₄

heterojunction formed by the one-pot annealing method. As shown in Fig. 8A, the reference Ce-CN-T sample shows lower photocatalytic activity ($201.7 \mu\text{mol}\cdot\text{h}^{-1}\cdot\text{g}^{-1}$) than the Ce-CN-5 sample ($292.5 \mu\text{mol}\cdot\text{h}^{-1}\cdot\text{g}^{-1}$). This may be due to limited visible light absorption ability of CeO_x ($E_g \sim 2.9 \text{ eV}$) without nitrogen doping as well as the much larger CeO_x nanoparticles hindering charge transfer and separation between $\text{g-C}_3\text{N}_4$ and CeO_x in Ce-CN-T (as evidenced by PL properties in Fig. 5 and Fig. 7). Moreover, the Ce-CN-M reference sample, with hydrogen production rate of only $142.5 \mu\text{mol}\cdot\text{h}^{-1}\cdot\text{g}^{-1}$, shows even much lower photocatalytic activity than Ce-CN-T, but close to pure $\text{g-C}_3\text{N}_4$. This may be because the mechanical method did not form $\text{CeO}_x/\text{g-C}_3\text{N}_4$ heterojunction with intimate interfacial contact due to serious aggregation of CeO_x nanoparticles, resulting in the very low efficiency of charge transfer and separation between the two components.

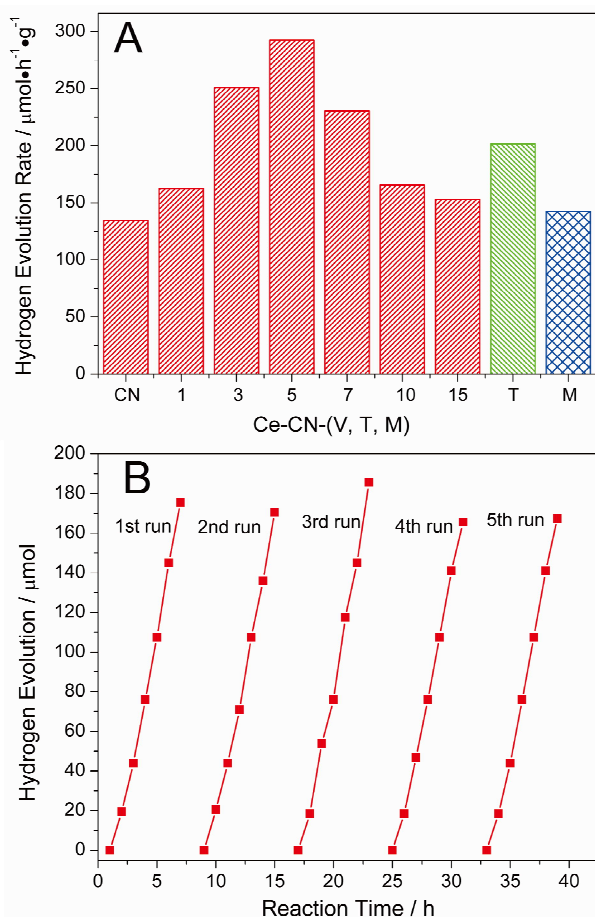


Fig.8 (A) Photocatalytic H_2 production under visible-light irradiation over $\text{g-C}_3\text{N}_4$, Ce-CN-V ($V = 1, 3, 5, 7, 10, 15$), Ce-CN-M and Ce-CN-T photocatalysts. T represents $\text{CeO}_x/\text{g-C}_3\text{N}_4$ (Ce-CN-T) prepared by the two-step method and M represents the mechanical mixture of CeO_x and $\text{g-C}_3\text{N}_4$ (Ce-CN-M). **(B)** Stable hydrogen evolution over Ce-CN-5 sample under visible light irradiation, the reactor was flushed with N_2 to evacuate the produced H_2 for every five hours.

To prove the existence and function of Pt nanoparticles as hydrogen evolution sites, TEM images for Pt loaded Ce-CN-5 after the photocatalytic hydrogen production reaction were taken, as shown in Fig. S9 in ESI†. Pt NPs with an average size of ca. 10 nm were only formed on the surface of $\text{g-C}_3\text{N}_4$ for both pure $\text{g-C}_3\text{N}_4$ and Ce-CN-5, indicating that Pt NPs preferred to be

reduced by the CB electrons from $\text{g-C}_3\text{N}_4$. That is to say, Pt NPs acted as the reduction active sites on $\text{g-C}_3\text{N}_4$ to entrap photoinduced electrons for photocatalytic hydrogen production, which has been evidenced by the previous studies.^{8,43,46-48}

As analyzed above, a possible photocatalytic mechanism of the as-prepared N- CeO_x NPs modified $\text{g-C}_3\text{N}_4$ nanocomposites for photocatalytic hydrogen production under visible light could be proposed and illustrated in Fig. 9. Upon visible light irradiation, both N- CeO_x and $\text{g-C}_3\text{N}_4$ were photo-excited to produce CB electrons and VB holes. Due to the VB and CB energy level difference between the two components, the CB electrons in N- CeO_x could easily transfer to the CB of $\text{g-C}_3\text{N}_4$ and then accumulated at Pt reduction active sites for H_2 production reaction; while the VB holes in $\text{g-C}_3\text{N}_4$ tended to transfer to the VB of N- CeO_x to react with the sacrificial reagent in the aqueous solution. In this Pt/N- $\text{CeO}_x/\text{g-C}_3\text{N}_4$ system, N- CeO_x acted as sensitizer improving light absorption and the Type II band alignment formed between N- CeO_x and $\text{g-C}_3\text{N}_4$ could efficiently separate the electron-hole pairs. Thus, the enhanced photocatalytic efficiency for hydrogen production under visible light was obtained over N- CeO_x NPs modified $\text{g-C}_3\text{N}_4$ when compared to pure $\text{g-C}_3\text{N}_4$.

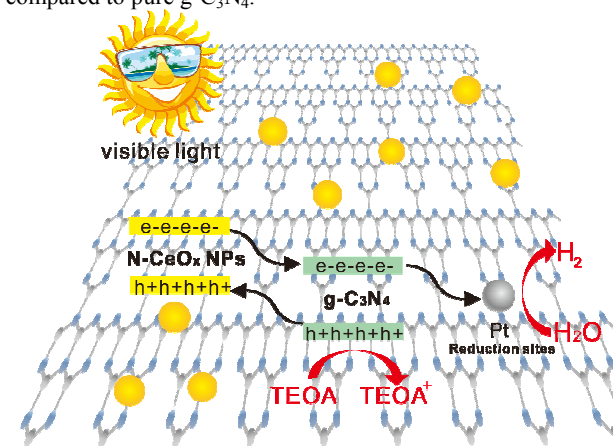


Fig.9 Schematic of band structure and charge transfer process in N- CeO_x NPs/ $\text{g-C}_3\text{N}_4$ for photocatalytic hydrogen generation.

Conclusions

Nitrogen-doped CeO_x nanoparticles modified $\text{g-C}_3\text{N}_4$ photocatalysts were successfully prepared via a one-pot annealing method. The photocatalytic activity for hydrogen production over $\text{g-C}_3\text{N}_4$ under visible light was greatly improved by nitrogen-doped CeO_x NPs modification. The photoactivity was enhanced by ~ 1.2 times, with hydrogen evolution rate increased from $134.5 \mu\text{mol}\cdot\text{h}^{-1}\cdot\text{g}^{-1}$ for pure $\text{g-C}_3\text{N}_4$ to $292.5 \mu\text{mol}\cdot\text{h}^{-1}\cdot\text{g}^{-1}$ for the optimized sample of nitrogen-doped CeO_x NPs modified $\text{g-C}_3\text{N}_4$ prepared by the one-pot method. It was believed that the greatly enhanced photocatalytic activity was mainly attributed to the improved visible light absorption with nitrogen-doped CeO_x NPs acting as sensitizers as well as the Type II band alignment induced efficient charge separation between nitrogen-doped CeO_x NPs and $\text{g-C}_3\text{N}_4$ with intimate interfacial contact. The present study put forward a new facile method for nitrogen doping and heterojunction formation in the meantime, which might open novel vistas for exploring nanostructured heterojunctions for photo(electro)catalytic and optoelectronic applications.

Acknowledgements

The authors gratefully acknowledge the financial supports from the National Natural Science Foundation of China (No. 51102194, No. 51323011, No.51121092), the Natural Science Foundation of Shaanxi Province (No. 2014KW07-02), the Natural Science Foundation of Jiangsu Province (No. BK20141212) and the Nano Research Program of Suzhou City (No. ZXG2013003). One of the authors (S. Shen) was supported by the Foundation for the Author of National Excellent Doctoral Dissertation of China (No. 201335) and the “Fundamental Research Funds for the Central Universities.”

Notes and references

^a International Research Centre for Renewable Energy, State Key Laboratory of Multiphase Flow in Power Engineering, Xi'an Jiaotong University, Shaanxi 710049, China. Fax: 86 82669033; Tel: 86 82668296; E-mail: shshen_xjtu@mail.xjtu.edu.cn (S. Shen), ljguo@mail.xjtu.edu.cn (L. Guo).

[†] Electronic Supplementary Information (ESI) available: The illustrations for fabrication and formation process of Ce-CN-V photocatalysts, particle size distribution histogram, XPS, DFT calculation results, UV-vis, PL spectra, TEM images and decay kinetics for the as-prepared photocatalysts. See DOI: 10.1039/b000000x/

- 1 K. Akihiko, M. Yugo, *Chem. Soc. Rev.*, 2009, **38**, 253–278.
- 2 K. Zhang, L. J. Guo, *Catal. Sci. Technol.*, 2013, **3**, 1672–1690.
- 3 X. Chen, S. Shen, L. Guo, S. S. Mao, *Chem. Rev.*, 2010, **110**, 6503–6570.
- 4 L. L. Amy, G. Q. Lu, T. Y. John, *Chem. Rev.*, 1995, **95**, 735–758.
- 5 P. Li, Z. Wei, T. Wu, Q. Peng, Y. D. Li, *J. Am. Chem. Soc.*, 2011, **133**, 5660–5663.
- 6 J. Fang, L. Xu, Z. Zhang, Y. Yuan, S. Cao, Z. Wang, L. S. Yin, Y. S. Liao, C. Xue, *ACS Appl. Mater. & Interfaces*, 2013, **5**, 8088–8092.
- 7 M. Kazuhiko, T. Tsuyoshi, H. Michikazu, S. Nobuo, I. Yasunobu, K. Hisayoshi, D. Kazunari, *J. Am. Chem. Soc.*, 2005, **127**, 8286–8287.
- 8 X. C. Wang, K. Maeda, A. Thomas, K. Takanabe, G. Xin, J. M. Carlsson, K. Domen, M. Antonietti, *Nat. Mater.*, 2009, **8**, 76–80.
- 9 X. C. Wang, B. Siegfried, A. Markus, *ACS Catal.*, 2012, **2**, 1596–1606.
- 10 J. Liang, Y. Zheng, J. Chen, J. D. Hulicova, M. Jaroniec, S. Z. Qiao, *Angew. Chem. Int. Ed.*, 2012, **51**, 3892–3896.
- 11 X. F. Chen, J. S. Zhang, X. Z. Fu, M. Antonietti, X. C. Wang, *J. Am. Chem. Soc.*, 2009, **131**, 11658–11659.
- 12 G. Liu, P. Niu, C. Sun, C. S. Smith, Z. G. Chen, G. M. Lu, H. M. Cheng, *J. Am. Chem. Soc.*, 2010, **132**, 11642–11648.
- 13 J. Fu, Y. L. Tian, B. B. Chang, F. N. Xi, X. P. Dong, *J. Mater. Chem.*, 2012, **22**, 21159–21166.
- 14 K. Maeda, X. Wang, Y. Nishihara, D. Lu, M. Antonietti, K. Domen, *J. Phys. Chem. C.*, 2009, **113**, 4940–4947.
- 15 H. Yan, H. Yang, *J. Alloy. Compd.*, 2011, **509**, 26–29.
- 16 Y. J. Wang, R. Shi, J. Lin, Y. F. Zhu, *Energy Environ. Sci.*, 2011, **4**, 2922–2929.
- 17 S. Ye, L. G. Qiu, Y. P. Yuan, Y. J. Zhu, J. Xia, J. F. Zhu, *J. Mater. Chem. A.*, 2013, **1**, 3008–3015.
- 18 M. Xu, L. Han, S. Dong, *ACS Appl. Mater. Interfaces*, 2013, **5**, 12533–12540.
- 19 A. Primo, T. Marino, A. Corma, R. Molinari, H. Garcia, *J. Am. Chem. Soc.*, 2011, **133**, 6930–6933.
- 20 S. Kundu, J. Ciston, S. D. Senanayake, D. A. Arena, E. Fujita, D. Stacchiola, L. Barrio, R. M. Navarro, J. L. G. Fierro, J. A. Rodriguez, *J. Phys. Chem. C.*, 2012, **116**, 14062–14070.
- 21 Y. Wang, B. Li, C. Zhang, L. Cui, S. Kang, X. Li, L. Zhou, *Appl. Catal. B: Environ.*, 2013, **130**, 277–284.
- 22 S. Hu, F. Zhou, L. Wang, J. Zhang, *Catal. Commun.*, 2011, **12**, 794–797.
- 23 N. Wetchakun, S. Chaiwichain, B. Inceesungvorn, K. Pingmuang, S. Phanichphant, A. I. Minett, J. Chen, *ACS Appl. Mater. Interfaces*, 2012, **4**, 3718–3723.
- 24 W. Li, S. Xie, M. Li, X. Ouyang, G. Cui, X. Lu, Y. Tong, *J. Mater. Chem. A.*, 2013, **1**, 4190–4193.

- 25 C. Mao, Y. Zhao, X. Qiu, J. Zhu, C. Burda, *Phys. Chem. Chem. Phys.*, 2008, **10**, 5633–5638.
- 26 A. B. Jorge, Y. Sakatani, C. Boissiere, C. Roberts, G. Sauthier, J. Fraxedas, C. Sanchez, A. Fuertes, *J. Mater. Chem.*, 2012, **22**, 3220–3226.
- 27 G. Zhang, J. Zhang, M. Zhang, X. Wang, *J. Mater. Chem.*, 2012, **22**, 8083–8091.
- 28 S. C. Yan, Z. S. Li, Z. G. Zou, *Langmuir*, 2009, **25**, 10397–10401.
- 29 G. Li, N. Yang, W. Wang, W. F. Zhang, *J. Phys. Chem. C.*, 2009, **113**, 14829–14833.
- 30 Q. Li, B. Yue, H. Iwai, T. Kako, J. H. Ye, *J. Phys. Chem. C.*, 2010, **114**, 4100–4105.
- 31 Y. Liu, G. Chen, C. Zhou, Y. Hu, D. Fu, J. Liu, Q. Wang, *J. Hazard. Mater.*, 2011, **190**, 75–80.
- 32 M. Y. Wang, L. Sun, Z. Q. Lin, J. H. Cai, K. P. Xie, C. J. Lin, *Energy Environ. Sci.*, 2013, **6**, 1211–1220.
- 33 Y. D. Hou, A. B. Laursen, J. S. Zhang, G. G. Zhang, Y. S. Zhu, X. C. Wang, S. Dahl, I. Chorkendorff, *Angew. Chem. Int. Ed.*, 2013, **52**, 3621–3625.
- 34 D. Sun, M. Gu, R. Li, S. Yin, X. Song, B. Zhao, C. Li, J. Li, Z. Feng, T. Sato, *Appl. Surf. Sci.*, 2013, **280**, 693–697.
- 35 A. Thomas, A. Fischer, F. Goettmann, M. Antonietti, J. O. Müller, R. Schlögl, J. M. Carlsson, *J. Mater. Chem.*, 2008, **18**, 4893–4908.
- 36 Y. J. Zhang, A. Thomas, M. Antonietti, X. C. Wang, *J. Am. Chem. Soc.*, 2008, **131**, 50–51.
- 37 Y. B. Li, H. M. Zhang, P. R. Liu, D. Wang, Y. Li, H. J. Zhao, *Small*, 2013, **9**, 3336–3344.
- 38 X. H. Li, X. C. Wang, M. Antonietti, *ACS Catal.*, 2012, **2**, 2082–2086.
- 39 R. Li, C. Fu, C. Q. Li, S. Yin, Y. Zhang, T. Sato, *J. Ceram. Soc. Jpn.*, 2010, **118**, 555–557.
- 40 V. Kumar, S. K. Sharma, T. P. Sharma, V. Singh, *Opt. Mater.*, 1999, **12**, 115–119.
- 41 J. Chen, S. Shen, P. Guo, M. Wang, P. Wu, X. Wang, L. Guo, *Appl. Catal. B: Environ.*, 2014, **152–153**, 335–341.
- 42 S. Shen, P. Guo, L. Zhao, Y. Du, L. Guo, *J. Solid State Chem.*, 2011, **184**, 2250–2256.
- 43 J. Chen, S. Shen, P. Guo, P. Wu, L. Guo, *J. Mater. Chem. A.*, 2014, **2**, 4605–4612.
- 44 D. R. Mullins, S. H. Overbury, D. R. Huntley, *Surf. Sci.*, 1998, **409**, 307–319.
- 45 J. Zhang, M. Zhang, R. Q. Sun, X. C. Wang, *Angew. Chem.*, 2012, **124**, 10292–10296.
- 46 J. Zhang, Q. Xu, Z. Feng, M. Li, C. Li, *Angew. Chem. Int. Ed.*, 2008, **47**, 1766–1769.
- 47 P. Gao, J. C. Liu, S. Lee, T. Zhang, D. D. Sun, *J. Mater. Chem.*, 2012, **22**, 2292–2298.
- 48 S. R. Lingampalli, U. K. Gautam, C. N. R. Rao, *Energy Environ. Sci.*, 2013, **6**, 3589–3594.